THE JOURNAL OF PHYSICAL CHEMISTRY Letters

Letter

Cite This: J. Phys. Chem. Lett. 2018, 9, 1237−1242

pubs.acs.org/JPCL

Isomeric Broadening of C_{60}^+ Electronic Excitation in Helium Droplets: Experiments Meet Theory

Alexander Kaiser, Johannes Postler, Milan Ončák, Martin Kuhn, Michael Renzler, Steffen Spieler, Malcolm Simpson, Michael Gatchell, Martin K. Beyer, Roland Wester, Francesco A. Gianturco, and Paul Scheier*

Institut für Ionenphysik und Angewandte Physik, Universität Innsbruck, Technikerstraße 25, A-6020 Innsbruck, Austria

Florent Calvo

University Grenoble Alpes, CNRS, LIPHY, F-38000 Grenoble, France

Ersin Yurtsever

Chemistry Department, Koç University, Rumeli Feneri Yolu, Sariyer 34450, Istanbul, Turkey

Supporting Information

ABSTRACT: Helium is considered an almost ideal tagging atom for cold messenger spectroscopy experiments. Although helium is bound very weakly to the ionic molecule of interest, helium tags can lead to shifts and broadenings that we recorded near 963.5 nm in the electronic excitation spectrum of C_{60}^+ solvated with up to 100 helium atoms. Dedicated quantum calculations indicate that the inhomogeneous broadening is due to different binding energies of helium to the pentagonal and hexagonal faces of C_{60}^+, their dependence on the electronic state, and the numerous isomeric structures that become available for intermediate coverage. Similar isomeric effects can be expected for optical spectra of most larger molecules surrounded by nonabsorbing weakly bound solvent molecules, a situation encountered in many messenger-tagging spectroscopy experiments.

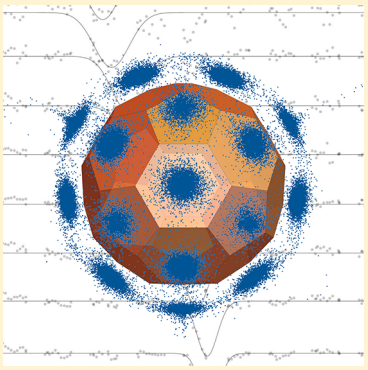

Messenger tagging, or the attachment of one or several weakly bound species to an ionic molecule of interest, is a powerful and increasingly widespread experimental technique to achieve high-resolution spectroscopy under cryogenic conditions in the gas phase and has been applied in atmospheric chemistry, for biologically relevant molecules, and in astrochemistry both in the infrared regime and for electronic excitations.[1−15] Using helium-messengers in a cryogenic ion trap, Campbell et al. have been able to identify C_{60}^+ as the origin of two diffuse interstellar bands by observing them in their laboratory experiments.[16] The only approximation made was an extrapolation from helium-covered cations to the bare cation. Helium is considered as an almost ideal tagging atom for action spectroscopy of molecular ions, and many experimental schemes that have been pioneered recently rely on helium messengers.[10,14,16−20] Its binding energy to most ions is so small that the He tags/adatoms boil off at very low excitation energies, its influence on the resonance position of electronic excitation of the dopant molecule is smaller than from other possible adatoms, and helium itself does not absorb below 20.6 eV. It therefore becomes an ideal nanoscopic probe for spectroscopy of molecular ions at low temperatures. However, even helium tagging leads to line-shifts and line-broadenings in absorptions, and extrapolation to bare spectra can be challenging.

As we have shown in our previous work, the preparation of helium solvated C_{60}^+ with up to 100 helium atoms has been achieved in helium nanodroplets.[21,22] The line-shifts of the two electronic absorption lines which were observed at around 957.9 and 963.5 nm were recorded for n = 1 up to n = 100 helium atoms, and a linear red-shift of about 0.7 Å per He atom was observed for n = 1 up to the commensurate coverage of all 12 pentagonal (5-rings) and 20 hexagonal (6-rings) faces at n = 32, followed by a more complex behavior indicative of a phase transition at larger sizes.[21] These line-shifts could be explained by a change in the spherical polarizability of C_{60}^+ upon excitation, together with the variety of positions of helium atoms obtained from a quantum-corrected classical molecular dynamics simulation.[21] At very cold temperatures, helium atoms can be effectively trapped in shallow potential energy

Received: January 16, 2018
Accepted: February 22, 2018
Published: February 22, 2018

DOI: 10.1021/acs.jpclett.8b00150
J. Phys. Chem. Lett. 2018, 9, 1237−1242

minima, and many possible isomers exist. The situation is still comparatively simple for fullerenes, where helium prefers adsorption sites above centers of 5-rings or 6-rings of carbon atoms, with small barriers in between.[23,24] For other molecules and in particular more complex biomolecules, the number and variety of possible microsolvated isomers can be much more complicated and will also depend on the cluster temperature and annealing conditions.

In the present work we show that the size-dependent broadening effects of the spectroscopic lines, despite being of small magnitude relative to the primary shifts, can be quantitatively interpreted as a consequence of isomeric broadening and the possibility for such quantum systems to explore multiple isomers at the low temperature of the experiments. The different messenger-isomers experience slightly different $He-C_{60}^+$ attraction between the electronic ground and excited states due to the charge redistribution upon excitation. This additional isomeric source of inhomogeneous broadening of electronic absorptions can play a role in many upcoming experiments in messenger-tagging electronic spectroscopy.

The electronic spectra of $He_nC_{60}^+$ ions were recorded by action spectroscopy as detailed in Experimental and Computational Methods. The spectra obtained for a set of representative clusters ranging in size from $n = 6$ to $n = 33$ are shown in Figure 1 and were each fitted using a single Gaussian profile.

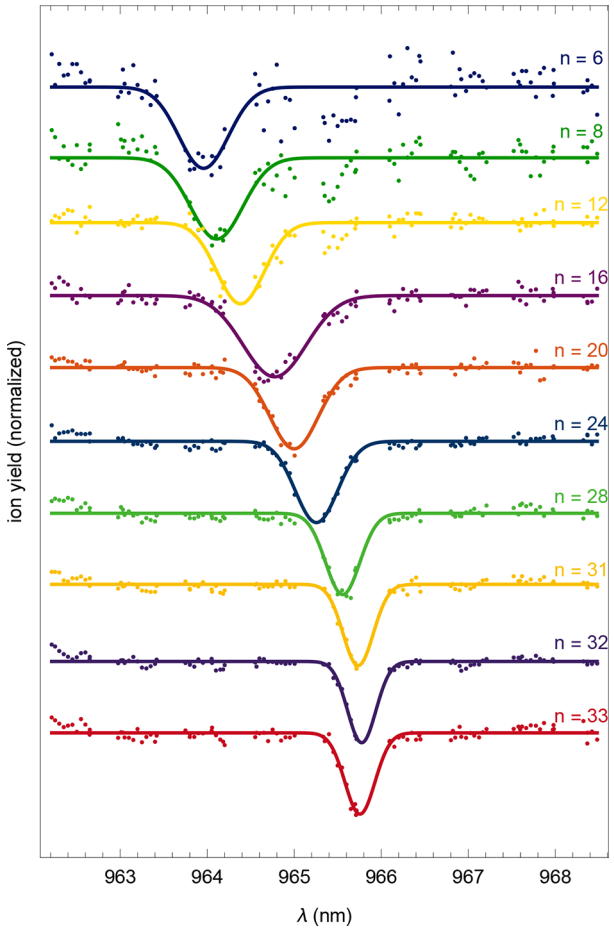

Figure 1. Ion signal for $He_nC_{60}^+$ as a function of laser wavelength with resonances that shift their position and change their width as a function of cluster size *n*.

The line-shift evident from the variation in the positions of the minima has previously been explained by helium binding differently to C_{60}^+ in the ground and excited electronic states, the latter having a slightly higher polarizability than the former.[21] Here we focus on the systematic changes in the broadenings, i.e., the full-width at half-maximum (fwhm) of the Gaussian fits that overlay the experimental data almost perfectly, and their origin. These widths are shown in Figure 2 in the range for $n = 5$ to $n = 60$ (blue triangles).

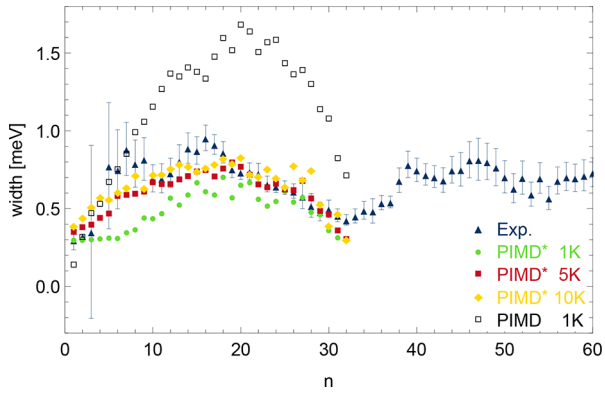

Figure 2. Theory meets experiment. The experimental broadenings (Exp.) in the first excitation energy of C_{60}^+ are compared to ground-state energetic broadening of $He_nC_{60}^+$ (PIMD 1K) and our model for isomeric broadening (PIMD*), as described in the text and by eq 2, for three different estimates of the cluster temperature.

The data below $n = 7$ suffers from low-quality detection due to overlap with ^{13}C isotopes of C_{60} and could not be used for $n < 5$. Instead, we include the results from Campbell et al. for $n = 1, 2, 3$ from similar experiments in a cold ion trap,[16,25,26] where these transitions are well-resolved. Although resolution is an issue for smaller clusters, clear trends are evident with a minimum for low occupation and another minimum for the commensurate phase at $n = 32$, where all faces of the fullerene are occupied with a single He atom. The width is largest for intermediate coverage and for high coverage ($n > 40$).

A series of calculations were performed to shed light on the molecular origins of the observed trends in the broadenings measured for $n = 1-32$. Very high-level excited-state calculations with sufficiently large basis sets are computationally not yet accessible for such large systems. In particular, accuracies for computed binding energies below the milli-electronvolt range cannot be realistically expected. Instead, a complete active-space self-consistent field (CASSCF) calculation was performed for bare C_{60}^+ taking into account only the h_u-g_g/h_g transition and the C_{2h} symmetry subgroup of I_h in MOLPRO.[27] A first excitation energy of 1.7 eV was obtained, which is considerably higher than the measured 1.287 eV of the 963.5 nm line; the deviation between experiment and theory is likely due to the neglect of dynamical electron correlation. However, owing to the high symmetry used in the calculation, the electron redistribution upon excitation should be rather well-described because it is known to be strongly symmetry-controlled. In Figure 3 an isosurface (isovalue 8.7×10^{-5} e/Å^3) of the electron density difference between the first excited state and the ground state is shown, corresponding to the h_u-h_g transition.

According to this calculation, upon excitation the electrons flow primarily from the inner side of 5-rings to the regions of

DOI: 10.1021/acs.jpclett.8b00150
J. Phys. Chem. Lett. 2018, 9, 1237−1242

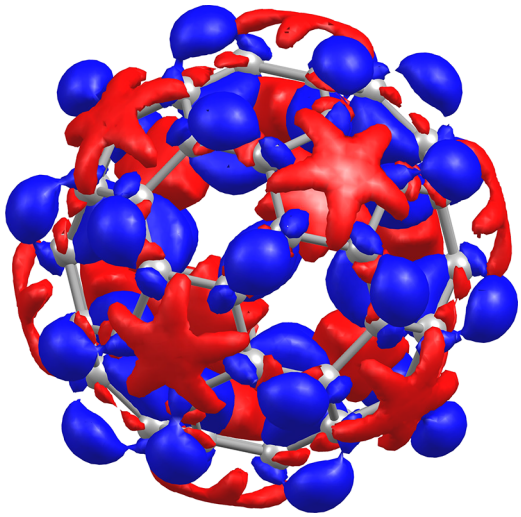

Figure 3. Calculated charge density differences between the first allowed excited state (h_g representation in the I_h symmetry group) and the ground state of C_{60}^+ (h_u representation in I_h). Differential electron accumulation upon excitation is shown in blue, while differential electron depletion is in red with respect to the distribution of the electronic ground state.

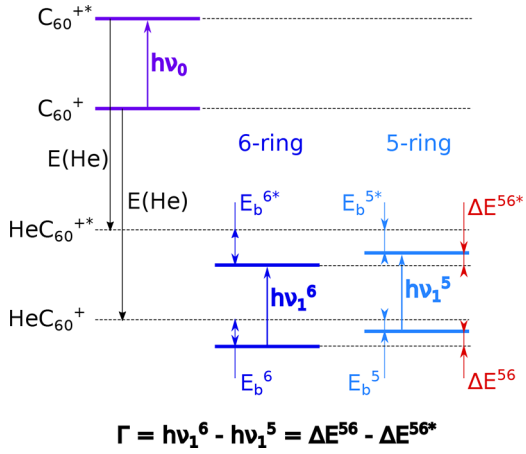

Figure 4. Pictorial view of the energy scheme of the ground and excited state of C_{60}^+ and HeC_{60}^+. The binding energy, E_b, between He and the two states of the fullerene leads to a shift in the average absorption frequency and to an isomeric broadening Γ which depends on the position of He that can be adsorbed on either a 5-ring or a 6-ring element. Energy scales were chosen for better readability and do not reflect the correct relative energies of the various states.

the 6−6 bonds. Such an electron redistribution can be expected to change the relative interaction strength of the He adatoms adsorbed near the 5-rings compared with those adsorbed near the 6-rings.

These findings indicate that a spherical polarizability model would be unable to correctly describe the subtle differences that clearly depend on anisotropic effects and the specific locations of helium adatoms. The He−C_{60}^+ binding energy dominates the shifts and will also dominate the broadening, at least under the assumption of a vertical excitation process with minor geometrical rearrangements. The relevant binding energy differs slightly depending on the position of He on C_{60}^+ for which the only locally stable binding sites are located above centers of 6-rings and 5-rings.[23] The energetic scheme of the adsorption process is pictorially outlined in Figure 4 for C_{60}^+ and HeC_{60}^+ for their ground and excited states.

In the ground state, the semiempirical model of ref 28 that is based on ab initio data[23] for neutral C_{60} predicts binding energies of 17 and 15.4 meV for helium on the 6-ring and 5-ring sites of C_{60}^+, respectively. The difference of 1.6 meV that is given for the ground state may change slightly when C_{60}^+ is electronically excited because of the electron redistribution that has been illustrated in Figure 3. These changes in binding energy affect the various $He_nC_{60}^+$ isomers in different ways.

Using now time-dependent density-functional theory, the first allowed excitation energy for HeC_{60}^+ can be estimated to be 1.4129 eV when He occupies the 6-ring and 1.4126 eV when He occupies the 5-ring, relative to the ground states. The difference of 0.3 meV is certainly smaller than the expected accuracy of the computations, but it gives an initial estimate of the order of magnitude and, more importantly, the sign of the effect. In other words, the adatom binding energy is changed by a small amount in favor of binding to 5-rings upon excitation of HeC_{60}^+, while the effect is not large enough to change the order of the preferred binding site in the excited state. We show below that this slight change can indeed be taken to be responsible for the size-dependent broadenings observed in the experiments.

Buckminsterfullerene C_{60} has 20 hexagonal and 12 pentagonal faces. If adsorption takes place only in the most favorable sites on 5-rings and 6-rings, the number of possible ways to draw m out of 20 and $n - m$ out of 12 is

$$N_I = \frac{1}{m!}\frac{20!}{(20-m)!}\cdot\frac{1}{(n-m)!}\frac{12!}{(12-n+m)!} \quad (1)$$

for a certain coverage n and accounting for He exchange symmetry but neglecting in a first approach the symmetry of C_{60}^+ so that some of the isomers are identical. Note that the C_{60}^+ symmetry can be lower than I_h because of the Jahn−Teller distortion.[29] Nevertheless, from a statistical viewpoint, the probability for occupying m 6-rings and $(n - m)$ 5-rings in $He_nC_{60}^+$ is given by N_I, which reaches its largest value for $n = 16$ and $m = 10$. The sum over all possible m for a given n provides the number of isomers for a specific $He_nC_{60}^+$ cluster which reaches its maximum value at $n = 16$ with ca. 6×10^8 isomers, again disregarding C_{60}^+ symmetry. For each value of n, we draw 50 random structures from the probability distribution $N_I(m)$ as inputs for the simulations.

With these initial conditions, path-integral molecular dynamics (PIMD) simulations were performed to solve numerically the nuclear Schrödinger equation for the motions of the helium atoms while the coordinates of the carbon atoms of C_{60}^+ were held fixed. The simulations yield the isomeric distribution of $He_nC_{60}^+$ in the electronic ground state. Twice the root-mean-square deviation of the raw distributions of quantum virial energies for all simulated isomers at 1 K are shown in Figure 2 (empty squares) in comparison with the experimental data. They clearly display a marked isomer effect that already resembles the experimental broadenings of the measured excitation energies. This ground-state isomeric effect comes from (a) the small differences in binding energy for the He-on-5-ring and He-on-6-ring interactions and (b) the He−He interaction that depends primarily on the number of close He atom neighbors for a particular isomer. However, assuming a vertical excitation scheme for the nuclei of the molecular cation (a realistic assumption for the present system), the excited state will be shifted by exactly the same He−He

DOI: 10.1021/acs.jpclett.8b00150
J. Phys. Chem. Lett. 2018, 9, 1237−1242

interaction that operates for the ground state; hence, the He−He interactions will not contribute to the relative shifts between two states. Following ref 21, we also tried to modify the spherical polarizability of C_{60}^+ by slightly changing the attractive part of the C−He interaction according to $\Delta\alpha$ = 18 a.u.; however, this modification turned out to have a vanishingly small isomer effect on PIMD energies and cannot explain sufficiently the experimental broadenings.

As described above, the relative strengths of the He-5-ring and the He-6-ring binding energies can change upon excitation, thus shifting differently the C_{60}^+ ground-state and the excited-state energies. To quantitatively estimate the influence of this effect, the number of He-on-5-rings was counted for each isomer and accumulated over time from the PIMD trajectories. For HeC_{60}^+, either one or zero 5-rings can be occupied, while for $He_2C_{60}^+$ we obtain a distribution for occupation of 2, 1, or 0 pentagons, and so on for larger number of He adatoms. Dissociation of He from the cluster is also an aspect to be considered, especially in the higher-temperature simulation at 10 K, and in the present modeling the dissociated trajectories were excluded from the isomer statistics because they would correspond to a different cluster size. Hence, we can design a new model that can now quantify the effect of the small changes in binding energies upon excitation by using an isomer-weighted sum over Lorentzian functions that are shifted for different isomers by the isomeric effect Γ (see also Figure 4). The individual Lorentzians have an intrinsic width γ, and the broadening as a function of n adatoms can then be obtained from the full width half-maximum of the sum over the Lorentzians that are shifted by the value of Γ times the number of occupied 5-rings:

$$\text{width}\,(n) = \text{fwhm}\left(\sum_j \frac{A(n,j)}{\frac{\gamma^2}{4} + (\nu - j\Gamma)^2}\right) \tag{2}$$

where $A(n, j)$ is the number of occurrences of occupation of j 5-rings in $He_nC_{60}^+$ taken from the PIMD simulations, and the sum runs over all 5-rings from 0 to 12. The intrinsic width γ was chosen from the experimental width of $He_{32}C_{60}^+$, which exists only as a single isomer, yielding a value of γ = 0.3 meV. The isomeric effect Γ was chosen to fit the increase in experimental broadening from $He_{32}C_{60}^+$ to $He_{31}C_{60}^+$ for the 5 K simulation, taking the value of Γ = 0.2 meV. Note that this choice is also very close to the calculated time-dependent density functional theory value of 0.3 meV mentioned above. Γ = 0.2 meV can also be inferred from the asymmetry in the broadening of $He_{1-3}C_{60}^+$ that has been measured by Campbell et al.[26] A very recent high-resolution measurement of the $He_1C_{60}^+$ absorption at 963.5 nm by Maier et al. also confirms its asymmetric line shape and is consistent with our value for Γ.[30] The two parameters appearing in eq 2 are thus all extracted from either experiments or directly from ab initio calculations. The use of eq 2 with isomer statistics from PIMD trajectories at 1, 2, and 5 K yields the width values shown in Figure 2, denoted by PIMD*. At lower temperatures more helium adatoms are located at the 6-rings and the isomeric effects are smaller than at higher temperatures. In Figure 2, the broadening of excitation lines (PIMD*) is smaller than the spread in ground-state energies (PIMD) because (a) PIMD* depends only on relative changes of the He on 5-ring and He on 6-ring interaction $\Delta E^{56} - \Delta E^{56*}$ and (b) He−He interactions do not contribute in the case of PIMD*, because we assume a vertical excitation process.

As can be seen from the data of Figure 2, this simple model can accurately explain the experimentally observed trends in the broadening of the 963.5 nm line, thus showing that the size dependence is due to nonmonotonic isomeric broadening. Each isomer has a narrow transition with the intrinsic width γ, but the unresolved isomeric splitting in energies results in a detectable systematic inhomogeneous broadening of the measured lines. The predicted temperature dependence of the isomeric effect shown in the present study may also provide a route toward realistic estimates of the actual cluster temperature given that the internal energy is sufficient to reach a thermal equilibrium in our 1, 5, and 10 K simulations. With stronger interacting adsorbate atoms or molecules, even stronger isomeric effects can be expected and may possibly explain some of the interesting features measured in ref 31 for Ne, Ar, Kr, H_2, D_2, and N_2 on C_{60}^+. In particular, we expect the isomeric effect Γ to depend on the structure and polarizability of the adsorbate particles and the isomeric distribution to depend on the cluster temperature, the relative adsorption energies on both 5-ring and 6-ring sites, and possibly the migration barrier between them that could cause metastable trapping. Also, planned experiments with hydrogen instead of helium could give insight into the role of vibronic coupling on the absorption lines.

EXPERIMENTAL AND COMPUTATIONAL METHODS

Helium-nanodroplets, with an average size of 2 × 10^5 He atoms, were doped with C_{60} in a pick-up cell and ionized via electron impact at 60 eV. The abundance distribution of $He_nC_{60}^+$ ions was recorded with a high-resolution reflectron time-of-flight mass spectrometer. Overlapping peaks for similar masses could be distinguished in an automated procedure using the IsotopeFit software.[32] Cluster cations were irradiated with a Ti:Sa cw laser Matisse TR from Sirah with 10 MHz bandwidth and ca. 0.6 W power. Laser-induced depletion of the ion yield at different mass-to-charge ratios was measured with the mass spectrometer while scanning the photon wavelength. Further details of this experiment can be found in refs 21 and 22.

In the CASSCF calculation of the h_u−h_g transition, 19 valence electrons were distributed over 10 active orbitals, i.e. (19, 10), allowing only for single excitations (further details are given in the Supporting Information). The Stuttgart double-ζ basis set and effective core potential were employed.[33]

The HeC_{60}^+ electronic excitation energies were also estimated using time-dependent density-functional theory with the B3LYP hybrid functional[34,35] and the triple-ζ basis set Def2-TZVP[36] within the *Gaussian 09* suite of programs.[37]

The PIMD method employed here ignores bosonic exchange effects, which are likely to be unimportant above 1 K owing to the much stronger binding of helium to the fullerene than to itself. The interactions between He and C atoms were modeled by including short-range Pauli repulsion, long-range dispersion, induction, and polarization forces. The functional form of the potential has been given earlier[28] and therefore will not be repeated here; it contains 5 parameters: A, B, C_6, C_8, and the isotropic polarizability α of helium. Each carbon atom carried a partial charge of $(1/60)e$, and the original parameters of this potential were derived from Varandas' calculations on the neutral HeC_{60} system.[23] Using MP2/aug-cc-pVTZ calculations for He attached to planar C_6^+ and C_5^+, two parameters of the

DOI: 10.1021/acs.jpclett.8b00150
J. Phys. Chem. Lett. 2018, 9, 1237−1242

Pauli repulsion have been rescaled so that the respective binding energies of the helium adatom to the 6-ring and 5-ring facets of C_{60}^+ are now 15.9 and 14.4 meV, respectively. The new set of parameters is given in the Supporting Information in Table 1S. Note that these binding energies refer to the electronic ground state of the cation.

As in ref 28, the He−He interactions were given by the accurate Janzen−Aziz potential,[38] and the PIMD trajectories were propagated at temperatures of 1, 5, and 10 K using massive Nosé−Hoover thermostats. The PIMD methodology has been described in detail elsewhere[39,40] and will not be repeated here. A Trotter number of 128 was chosen at all temperatures with time steps of 5 fs (1 and 5 K) and 1 fs (10 K) and simulation times of 100 ps for equilibration and 500 ps for production runs. With these values, the sampling of the phase space was found to be converged with no significant deviation in the distribution of isomers upon increasing the employed statistics. The He centroid positions accumulated for a specific $He_{12}C_{60}^+$ trajectory are depicted in Figure 1S, and the trajectories of selected helium atoms from $He_{12}C_{60}^+$, projected in the plane of spherical angles, are shown in Figure 2S. Helium is clearly delocalized and can change its binding sites quite often. Most of the time, however, individual helium atoms are located near the 6-ring centers or the 5-ring centers, with rare excursions between them.

■ ASSOCIATED CONTENT

Supporting Information

The Supporting Information is available free of charge on the ACS Publications website at DOI: 10.1021/acs.jpclett.8b00150.

Further details of the CASSCF calculations; graphical representation of a $He_{12}C_{60}^+$ PIMD trajectory (Figure 1S); 2D projection of the $He_{12}C_{60}^+$ PIMD trajectory (Figure 2S); parameters of the He−C interaction potential (Table 1S) (PDF)

■ AUTHOR INFORMATION

Corresponding Author

*E-mail: paul.scheier@uibk.ac.at.

ORCID

Alexander Kaiser: 0000-0002-9439-9176
Martin K. Beyer: 0000-0001-9373-9266
Roland Wester: 0000-0001-7935-6066
Paul Scheier: 0000-0002-7480-6205
Florent Calvo: 0000-0002-3621-3046

Notes

The authors declare no competing financial interest.

■ ACKNOWLEDGMENTS

This study was supported by the Austrian Science Fund (FWF) Projects P26635, W1259-N27, P28979-N27, M2001-NBL; by the European Union's Horizon 2020 research and innovation programme under Grant Agreement No. 692335; and by the Swedish Research Council (Grant Number 2016-06625). The computational results presented have been achieved using the HPC infrastructure at the Koç University and LEO3 of the University of Innsbruck.

■ REFERENCES

(1) Okumura, M.; Yeh, L. I.; Myers, J. D.; Lee, Y. T. Infrared spectra of the cluster ions $H_7O_3^+ \cdot H_2$ and $H_9O_4^+ \cdot H_2$. *J. Chem. Phys.* **1986**, *85*, 2328−2329.

(2) Bieske, E. J.; Dopfer, O. High-Resolution Spectroscopy of Cluster Ions. *Chem. Rev.* **2000**, *100*, 3963−3998.

(3) Robertson, W. H.; Johnson, M. A. Molecular aspects of ion hydration: The cluster approach. *Annu. Rev. Phys. Chem.* **2003**, *54*, 173−213.

(4) Headrick, J. M.; Diken, E. G.; Walters, R. S.; Hammer, N. I.; Christie, R. A.; Cui, J.; Myshakin, E. M.; Duncan, M. A.; Johnson, M. A.; Jordan, K. D. Spectral Signatures of Hydrated Proton Vibrations in Water Clusters. *Science* **2005**, *308*, 1765−1769.

(5) Polfer, N. C.; Oomens, J. Vibrational spectroscopy of bare and solvated ionic complexes of biological relevance. *Mass Spectrom. Rev.* **2009**, *28*, 468−494.

(6) Douberly, G. E.; Walters, R. S.; Cui, J.; Jordan, K. D.; Duncan, M. A. Infrared Spectroscopy of Small Protonated Water Clusters, $H^+(H_2O)_n$ (n = 2−5): Isomers, Argon Tagging, and Deuteration. *J. Phys. Chem. A* **2010**, *114*, 4570−4579.

(7) Leavitt, C. M.; Wolk, A. B.; Fournier, J. A.; Kamrath, M. Z.; Garand, E.; Van Stipdonk, M. J.; Johnson, M. A. Isomer-Specific IR−IR Double Resonance Spectroscopy of D_2-Tagged Protonated Dipeptides Prepared in a Cryogenic Ion Trap. *J. Phys. Chem. Lett.* **2012**, *3*, 1099−1105.

(8) Redwine, J. G.; Davis, Z. A.; Burke, N. L.; Oglesbee, R. A.; McLuckey, S. A.; Zwier, T. S. A novel ion trap based tandem mass spectrometer for the spectroscopic study of cold gas phase polyatomic ions. *Int. J. Mass Spectrom.* **2013**, *348*, 9−14.

(9) Jašík, J.; Žabka, J.; Roithová, J.; Gerlich, D. Infrared spectroscopy of trapped molecular dications below 4K. *Int. J. Mass Spectrom.* **2013**, *354*−*355*, 204−210.

(10) Chakrabarty, S.; Holz, M.; Campbell, E. K.; Banerjee, A.; Gerlich, D.; Maier, J. P. A Novel Method to Measure Electronic Spectra of Cold Molecular Ions. *J. Phys. Chem. Lett.* **2013**, *4*, 4051−4054.

(11) Wolk, A. B.; Leavitt, C. M.; Garand, E.; Johnson, M. A. Cryogenic Ion Chemistry and Spectroscopy. *Acc. Chem. Res.* **2014**, *47*, 202−210.

(12) Marsh, B. M.; Zhou, J.; Garand, E. Vibrational spectroscopy of isolated copper(ii) complexes with deprotonated triglycine and tetraglycine peptides. *RSC Adv.* **2015**, *5*, 1790−1795.

(13) Heine, N.; Asmis, K. R. Cryogenic ion trap vibrational spectroscopy of hydrogen-bonded clusters relevant to atmospheric chemistry. *Int. Rev. Phys. Chem.* **2015**, *34*, 1−34.

(14) Günther, A.; Nieto, P.; Müller, D.; Sheldrick, A.; Gerlich, D.; Dopfer, O. BerlinTrap: A new cryogenic 22-pole ion trap spectrometer. *J. Mol. Spectrosc.* **2017**, *332*, 8−15.

(15) Masellis, C.; Khanal, N.; Kamrath, M. Z.; Clemmer, D. E.; Rizzo, T. R. Cryogenic Vibrational Spectroscopy Provides Unique Fingerprints for Glycan Identification. *J. Am. Soc. Mass Spectrom.* **2017**, *28*, 2217−2222.

(16) Campbell, E. K.; Holz, M.; Gerlich, D.; Maier, J. P. Laboratory confirmation of C_{60}^+ as the carrier of two diffuse interstellar bands. *Nature* **2015**, *523*, 322−323.

(17) Johnson, C. J.; Wolk, A. B.; Fournier, J. A.; Sullivan, E. N.; Weddle, G. H.; Johnson, M. A. Communication: He-tagged vibrational spectra of the SarGlyH$^+$ and $H^+(H_2O)_{2,3}$ ions: Quantifying tag effects in cryogenic ion vibrational predissociation (CIVP) spectroscopy. *J. Chem. Phys.* **2014**, *140*, 221101.

(18) Masson, A.; Williams, E. R.; Rizzo, T. R. Molecular hydrogen messengers can lead to structural infidelity: A cautionary tale of protonated glycine. *J. Chem. Phys.* **2015**, *143*, 104313.

(19) Roithová, J.; Gray, A.; Andris, E.; Jašík, J.; Gerlich, D. Helium Tagging Infrared Photodissociation Spectroscopy of Reactive Ions. *Acc. Chem. Res.* **2016**, *49*, 223−230.

(20) Brünken, S.; Kluge, L.; Stoffels, A.; Pérez-Ríos, J.; Schlemmer, S. Rotational state-dependent attachment of He atoms to cold molecular

DOI: 10.1021/acs.jpclett.8b00150
J. Phys. Chem. Lett. 2018, 9, 1237−1242

ions: An action spectroscopic scheme for rotational spectroscopy. *J. Mol. Spectrosc.* **2017**, *332*, 67−78.
(21) Kuhn, M.; Renzler, M.; Postler, J.; Ralser, S.; Spieler, S.; Simpson, M.; Linnartz, H.; Tielens, A. G. G. M.; Cami, J.; Mauracher, A.; Wang, Y.; Alcamí, M.; Martín, F.; Beyer, M. K.; Wester, R.; Lindinger, A.; Scheier, P. Atomically resolved phase transition of fullerene cations solvated in helium droplets. *Nat. Commun.* **2016**, *7*, 13550.
(22) Spieler, S.; Kuhn, M.; Postler, J.; Simpson, M.; Wester, R.; Scheier, P.; Ubachs, W.; Bacalla, X.; Bouwman, J.; Linnartz, H. C_{60}^+ and the Diffuse Interstellar Bands: An Independent Laboratory Check. *Astrophys. J.* **2017**, *846*, 168.
(23) Varandas, A. J. C. Helium-fullerene pair interactions: An ab initio study by perturbation theory and coupled cluster methods. *Int. J. Quantum Chem.* **2011**, *111*, 416−429.
(24) Leidlmair, C.; Wang, Y.; Bartl, P.; Schöbel, H.; Denifl, S.; Probst, M.; Alcamí, M.; Martín, F.; Zettergren, H.; Hansen, K.; Echt, O.; Scheier, P. Structures, Energetics, and Dynamics of Helium Adsorbed on Isolated Fullerene Ions. *Phys. Rev. Lett.* **2012**, *108*, 076101.
(25) Campbell, E. K.; Holz, M.; Maier, J. P.; Gerlich, D.; Walker, G. A. H.; Bohlender, D. Gas Phase Absorption Spectroscopy of C_{60}^+ and C_{70}^+ in a Cryogenic Ion Trap: Comparison with Astronomical Measurements. *Astrophys. J.* **2016**, *822*, 17.
(26) Campbell, E. K.; Holz, M.; Maier, J. P. C_{60}^+ in Diffuse Clouds: Laboratory and Astronomical Comparison. *Astrophys. J., Lett.* **2016**, *826*, L4.
(27) Werner, H.-J.; Knowles, P. J.; Knizia, G.; Manby, F. R.; Schütz, M.; Celani, P.; Györffy, W.; Kats, D.; Korona, T.; Lindh, R.; Mitrushenkov, A.; Rauhut, G.; Shamasundar, K. R.; Adler, T. B.; Amos, R. D.; Bernhardsson, A.; Berning, A.; Cooper, D. L.; Deegan, M. J. O.; Dobbyn, A. J.; Eckert, F.; Goll, E.; Hampel, C.; Hesselmann, A.; Hetzer, G.; Hrenar, T.; Jansen, G.; Köppl, C.; Liu, Y.; Lloyd, A. W.; Mata, R. A.; May, A. J.; McNicholas, S. J.; Meyer, W.; Mura, M. E.; Nicklass, A.; O'Neill, D. P.; Palmieri, P.; D., P; Pflüger, K.; Pitzer, R.; Reiher, M.; Shiozaki, T.; Stoll, H.; Stone, A. J.; Tarroni, R.; Thorsteinsson, T.; Wang, M. *MOLPRO*, version 2015.1, a package of ab initio programs; 2015.
(28) Calvo, F. Size-induced melting and reentrant freezing in fullerene-doped helium clusters. *Phys. Rev. B: Condens. Matter Mater. Phys.* **2012**, *85*, 060502.
(29) Ramanantoanina, H.; Muya, J. T.; Ceulemans, A.; Daul, C. C_{60}^+ and B_{80}^+: A Comparative Study of the Jahn-Teller Effect. *J. Phys.: Conf. Ser.* **2013**, *428*, 012005.
(30) Maier, J. P.; Campbell, E. K. In preparation according to private communication, 2017.
(31) Holz, M.; Campbell, E. K.; Rice, C. A.; Maier, J. P. Electronic absorption spectra of C_{60}^+−L (L = He, Ne, Ar, Kr, H_2, D_2, N_2) complexes. *J. Mol. Spectrosc.* **2017**, *332*, 22−25.
(32) Ralser, S.; Postler, J.; Harnisch, M.; Ellis, A. M.; Scheier, P. Extracting cluster distributions from mass spectra: IsotopeFit. *Int. J. Mass Spectrom.* **2015**, *379*, 194−199.
(33) Bergner, A.; Dolg, M.; Küchle, W.; Stoll, H.; Preuß, H. Ab initio energy-adjusted pseudopotentials for elements of groups 13−17. *Mol. Phys.* **1993**, *80*, 1431−1441.
(34) Becke, A. D. Density-functional thermochemistry. III. The role of exact exchange. *J. Chem. Phys.* **1993**, *98*, 5648.
(35) Lee, C.; Yang, W.; Parr, R. G. Development of the Colle-Salvetti correlation-energy formula into a functional of the electron density. *Phys. Rev. B: Condens. Matter Mater. Phys.* **1988**, *37*, 785−789.
(36) Weigend, F.; Ahlrichs, R. Balanced basis sets of split valence, triple zeta valence and quadruple zeta valence quality for H to Rn: Design and assessment of accuracy. *Phys. Chem. Chem. Phys.* **2005**, *7*, 3297−3305.
(37) Frisch, M. J.; Trucks, G. W.; Schlegel, H. B.; Scuseria, G. E.; Robb, M. A.; Cheeseman, J. R.; Scalmani, G.; Barone, V.; Mennucci, B.; Petersson, G. A.; Nakatsuji, H.; Caricato, M.; Li, X.; Hratchian, H. P.; Izmaylov, A. F.; Bloino, J.; Zheng, G.; Sonnenberg, J. L.; Hada, M.; Ehara, M.; Toyota, K.; Fukuda, R.; Hasegawa, J.; T., M. I. a; Nakajima; Honda, Y.; Kitao, O.; Nakai, H.; Vreven, T.; Montgomery, J. A.; Peralta, J. E.; Ogliaro, F.; Bearpark, M.; Heyd, J. J.; Brothers, E.; Kudin, K. N.; Staroverov, V. N.; Kobayashi, R.; Normand, J.; Raghavachari, K.; Rendell, A.; Burant, J. C.; Iyengar, S. S.; Tomasi, J.; Cossi, M.; Rega, N.; Millam, J. M.; Klene, M.; Knox, J. E.; Cross, J. B.; Bakken, V.; Adamo, C.; Jaramillo, J.; Gomperts, R.; Stratmann, R. E.; Yazyev, O.; Austin, A. J.; Cammi, R.; Pomelli, C.; Ochterski, J. W.; Martin, R. L.; Morokuma, K.; Zakrzewski, V. G.; Voth, G. A.; Salvador, P.; Dannenberg, J. J.; Dapprich, S.; Daniels, A. D.; Farkas, Ö.; Foresman, J. B.; Ortiz, J. V.; Cioslowski, J.; Fox, D. J. *Gaussian 09*, revision A.1. Gaussian Inc.: Wallingford, CT, 2009.
(38) Janzen, A. R.; Aziz, R. A. An accurate potential energy curve for helium based on ab initio calculations. *J. Chem. Phys.* **1997**, *107*, 914−919.
(39) Calvo, F. Coating Polycyclic Aromatic Hydrocarbon Cations with Helium Clusters: Snowballs and Slush. *J. Phys. Chem. A* **2015**, *119*, 5959−5970.
(40) Calvo, F.; Yurtsever, E. Solvation of carbonaceous molecules by para-H_2 and ortho-D_2 clusters. I. Polycyclic aromatic hydrocarbons. *J. Chem. Phys.* **2016**, *144*, 224302.

DOI: 10.1021/acs.jpclett.8b00150
J. Phys. Chem. Lett. 2018, 9, 1237−1242